DESIGN OF BEAM DIAGNOSTIC SYSTEM FOR OPTICAL STOCHASTIC COOLING AT IOTA RING*

K. Yonehara†, Fermilab, Batavia, IL 60510, USA

Abstract

Design of beam diagnostic system for Optical Stochastic Cooling (OSC) at IOTA ring is described in the document. Cooling parameter will be measured by the longitudinal interference pattern of synchrotron radiation lights from two undulators. Light optics and detector system are discussed.

INTRODUCTION

Damping rate of the stochastic cooling (τ^{-1}) is proportional to the bandwidth of the electromagnetic wave (W) and the beam bunch length (σ_s), i.e. $\frac{1}{\tau} \propto W\sigma_s$. It indicates that Optical Stochastic Cooling (OSC) has a great potential to cool TeV-scale proton beams, e.g. LHC and FCC because the bandwidth of radiation lights is typically $\sim 10^{14}$ Hz (wavelength of radiation lights is $\lambda \sim \mu m$) which is four or five orders of magnitude higher (shorter) than a microwave that is used in the conventional stochastic device.

Theoretical investigation of the OSC has been done [1]. Here, several critical formulae are picked up for our discussion. Damping force applies to the longitudinal phase space. The force ($\delta p/p$) is tuned by the path length (Δs) that is adjusted by a chicane,

$$\delta p/p = \kappa \sin(k\Delta s), \tag{1}$$

where κ is the undulator strength and k is the wavenumber of a radiation light. The longitudinal kick is partitioned into the horizontal phase space (x) due to dispersion. To evaluate the stochastic process, the force is averaged along the beam path in a whole ring lattice. It is given as

$$F_1(a_x, a_p) = 2J_0(a_p)J_1(a_x)/a_x, \tag{2}$$

$$F_2(a_x, a_p) = 2J_0(a_x)J_1(a_p)/a_p, \tag{3}$$

where J_0 and J_1 are the 0-th and 1-st order Bessel functions, respectively. a_x and a_p are the dimensionless amplitude that represents the phase advance of beams in the kicker undulator in horizontal (x) and longitudinal (s) phase spaces, respectively. In order to realize the positive average damping force, the phase advance between the beam and the kicker light should be $|a_x, a_p| < \mu_{01} \sim 2.405$.

Proof-of-principle experiment will be done at IOTA ring in Fermilab by using an electron beam. Figure 2 is a layout of cooling insert at IOTA ring. No optical amplifier is used in the first test. Table 1 shows the main beam parameter and the beam optics parameter in the cooling insert at IOTA ring. Dipole and quadrupole magnets are a main tuning knob to adjust the beam path length. A sextupole magnet is applied in the beam line to increase the acceptance by correcting the chromaticity. It significantly changes the path length, thus it changes the cooling condition as shown in Fig. 3. Major goal of the designed beam diagnostic system is to measure the beam path length as a function of the sextupole field strength and to observe this correlation.

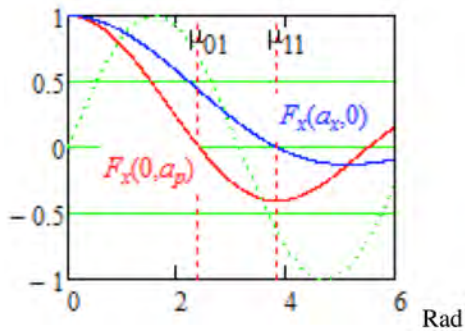

Figure 1: Averaged damping forces.

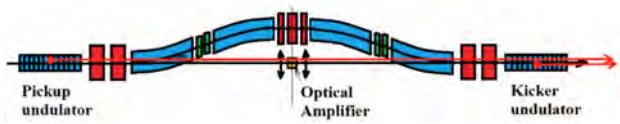

Figure 2: A cooling insert for the OSC in IOTA ring. The blue box is a bending magnet. The red and green boxes are a quadrupole and a sextupole magnets, respectively. The orange line shows a path of a synchrotron radiation light.

Table 1: Beam Parameter

IOTA ring	
Circumference	40 m
Nominal electron beam energy	100 MeV
Bending field of main dipoles	4.8 kG
Revolution	7.5 MHz
Undulators	
Radiation wavelength at zero angle, $\lambda_{\gamma,0}$	2.2 μ m
Undulator parameter	0.8
Undulator period	12.9 cm
Number of periods	6
Total undulator length	0.77 m
Peak magnetic field	664 G
Distance between centers of undulators	3.3 m
Energy loss per undulator per pass	22 meV
Optical system aperture	13 mm
Radiation spot size in the kicker, HWHM	0.35 mm
θ_{max}	4 mrad
$\gamma\theta_{max}$	0.63

* Work supported by Fermilab Research Alliance, LLC under Contract No. DE-AC02-07CH11359

† yonehara@fnal.gov

ISBN 978-3-95450-174-8

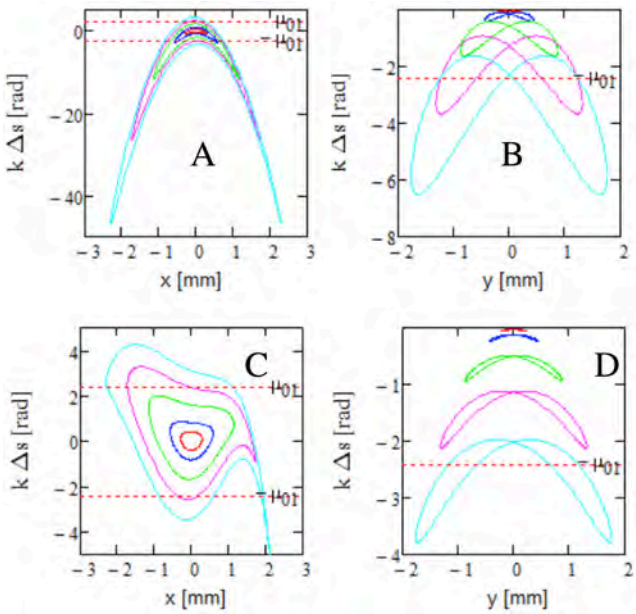

Figure 3: (Left) beam path length as a function of horizontal beam position without (A) and with (C) a sextupole magnet. (Right) beam path length as a function of vertical beam position without (B) and with (D) a sextupole magnet.

Table 2: Cooling Parameters

Cooling parameter	
Radiation band	2.2 - 3.2 μ m
Damping rate (x/s)	6.3/5.2 s^{-1}
RMS bunch length (no OSC)	22 cm
Number of particles per bunch	10^6

DESIGN OPTICS FOR SYNCHROTRON RADIATION IN UNDULATOR

Optical transport for the synchrotron radiation light is discussed. Primary goal of the design of transport optics is maintaining the phase space of object (synchrotron radiation lights) in the pickup undulator to the image in the kicker undulator. Then, two lights are extracted from the beam line to use for the beam diagnostics.

Synchrotron Radiation from Undulator

First, the synchrotron radiation light produced in the undulator is characterized. By taking into account the angular dependent Doppler shift, there is a strong correlation between spectrum and angular distribution of synchrotron light, which is given

$$\lambda_\gamma = \frac{\lambda_p}{2\gamma^2}\left(1+\gamma^2\left(\frac{1}{2}\theta_e^2+\theta^2\right)\right) = \lambda_{\gamma,0}+\frac{\lambda_p}{2}\theta^2, \quad (4)$$

where $\lambda_{\gamma,0}$ is the shortest wavelength at zero radiation angle emitted in the pickup undulator. According to the diffraction limit, the angular distribution of synchrotron light from an undulator is restricted by $\theta \sim 1/\gamma$ [2]. Therefore, the second term in eq. (4) is given

$$\frac{\lambda_p}{2}\theta^2 \equiv \Delta\lambda \sim \frac{\lambda_p}{2\gamma^2}. \quad (5)$$

Figure 4 shows the estimated wavelength as a function of the conical angle from the light source. Because the optical system aperture is 13 mm and the gap between two undulators is 3.3 m the geometric acceptance of the radiation light is ~4 mrad. It limits the longest wavelength of radiation ~3.2 μm.

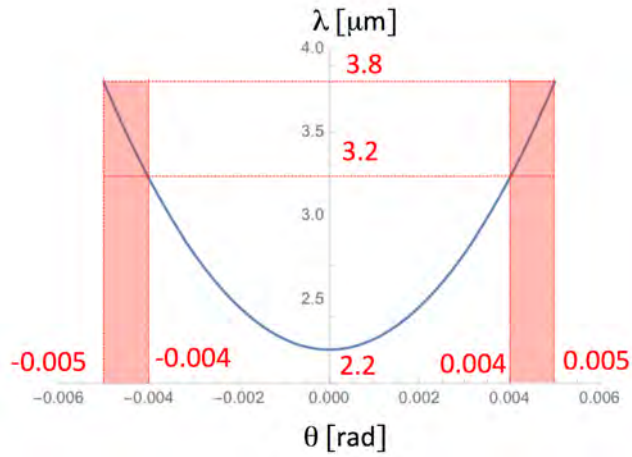

Figure 4: Spectrum of synchrotron light from the pickup undulator. A red area is the boundary of optical aperture.

Transfer Matrix of Synchrotron Radiation

A triplet lens is applied. A transfer matrix of the triplet lens with the paraxial optics model is

$$F_1 = \begin{bmatrix} 1 & 0 \\ \frac{1}{f_1} & 1 \end{bmatrix}, F_2 = \begin{bmatrix} 1 & 0 \\ \frac{1}{f_2} & 1 \end{bmatrix}, T = \begin{bmatrix} 1 & t \\ 0 & 1 \end{bmatrix}, L = \begin{bmatrix} 1 & l \\ 0 & 1 \end{bmatrix}, \quad (6)$$

$$M = L.F_1.T.F_2.T.F_1.L, \quad (7)$$

where f_1 is a focal length of the first and third lenses while f_2 is a focal length of the middle one. t is a gap between F_1 and F_2, and F_2 and F_1. l is a gap between the middle point of the pickup undulator and the first F_1, and the second F_1 to the middle point of the kicker undulator. In order to maintain the phase space of source object in the pickup undulator to the kicker one, the transfer matrix should be the identity matrix, $M = \pm I$. f_1 and f_2 are the function of t,

$$f_1^{-1} = -\frac{1}{t}, \quad f_2^{-1} = \frac{1}{t}. \quad (8)$$

The result shows that the focal length is independent from l.

Ray Trace Simulation

Ray trace simulation has been done by using a custom made code based on LensLab [3]. Geometry and refraction index of lenses are modeled from real lens. Figure 5 shows an example of ray tracing in a triplet lens.

ISBN 978-3-95450-174-8

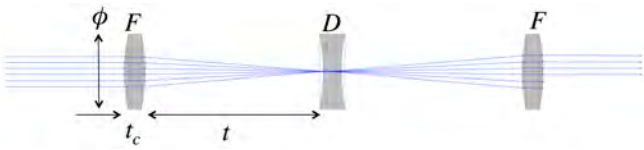

Figure 5: Demonstration of a triplet lens.

Because the focal length is independent from l the displacement of light source (object) from the center of pickup undulator is maintained to the displacement of the image from the center of kicker undulator. Figure 6 verifies this concept.

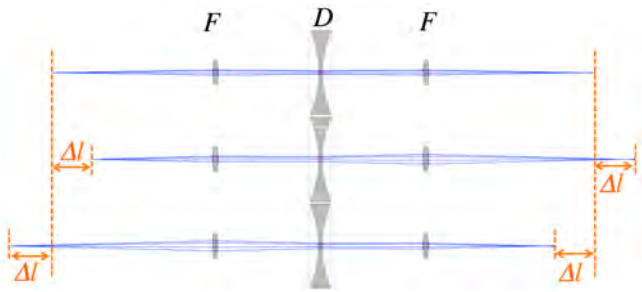

Figure 6: Longitudinal displacement of the object and the image in the triplet lens. Transverse displacement of the object is also maintained in the triplet lens although it does not show in this figure.

Table 3 shows the geometry of lens what we used in the simulation. The values are picked up from a catalog provided by Melles Griot [4]. We assume that the glass material is a standard BK7. It is important to point out that the total amount of glass should be ~6 mm because the time of flight of radiation light must synchronize to the electron beam. The present lens design is close enough to the requirement.

Table 3: Cooling Parameters

Element	Focal length f	Diameter ϕ	Thickness t_c
Unit	mm	mm	mm
F_1	50	12.5	2.8
F_2	-50	42.0	2.0

Figure 7 shows the simulated image spot in the kicker undulator produced by single electron in ray trace simulation. Largest radius (λ = 3.2 μm) is 65 nm in this analysis. On the other hand, the estimated spot size from the diffraction limit is $\sigma_x \sim R(1-\cos\theta) \sim R(1-\cos\gamma^{-1}) \sim 5$ μm in this undulator where R is a bending radius in the undulator. Besides, the beam size is a couple of hundreds of μm. Therefore, the chromaticity is not an issue in this system.

DESIGN OF BEAM DIAGNOSTIC SYSTEM

It is essential to demonstrate the cooling performance by tuning the sextuple magnet. The longitudinal interference pattern will be observed to measure the phase-offset. In case of the single electron, the longitudinal interference pattern is given,

$$1 + \exp(i\delta) = 2\cos^2\left(\frac{\delta}{2}\right), \quad (9)$$

where δ is the phase offset between the electron and synchrotron light in the kicker undulator. The power of two synchrotron lights will be changed as sinusoidal function with respect to the phase offset. This approximation is valid when the synchrotron light is coherent. As the next step, time structure of the beam and beam quality has been involved in ray trace simulation to investigate the coherence of synchrotron lights.

An electron beam is oscillated in horizontal plane in the undulator and emit near-infrared linearly polarized lights. Since an electron loses energy by 22 meV every passing in the undulator the production rate of photons are $\Delta\varepsilon/h\nu \sim 0.04$. Revolution of beams are 7.5 MHz. Therefore, the total number of photons are $0.04\times10^6\times7.5\cdot10^6 \sim 3\cdot10^{11}$ photons/sec. Figure 8 shows the schematic of beam diagnostic system. Synchrotron radiation lights are extracted from the beam line through a viewer. The lights is filtered by a band-pass filter to select the short narrow-band light. They take a part by a splitter. One goes into a photo detector array to measure the spatial distribution and other goes into a fast photo detector to measure the interference light.

There are several Near-IR photon detectors. HgCdTe PEM-detector is the standard semiconductor NIR photon detector. It can be very fast rise time (τ << 1 ns) and the total pulse width is 3~4 ns. This should be applicable for the time domain single photon counter. On the other hand, a superconducting nano-wire bolometer has been developed for the single NIR photon counter. This is also very fast rise time ($\tau \sim 10$ ps) but it has a long recovery time. It can achieve a very fine spatial resolution, order of μm. The superconducting bolometer needs a cryogenics.

REFERENCES

[1] V. Lebedev, *"Optical Stochastic Cooling"*, *ICFA News Letter* **65** (2014) 100.

[2] K.J. Kim, *"Angular Distribution of Undulator Power for an Arbitrary Deflection Parameter K"*, *Nucl. Inst. Meth.* **A246** (1986) 67.

[3] *http://library.wolfram.com/infocenter/MathSource/655/.*

[4] *http://mellesgriot.com/.*

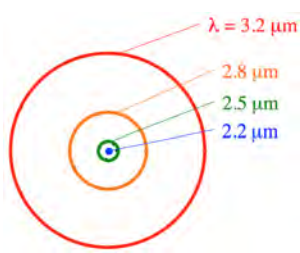

Figure 7: Simulated image spot at the center of kicker undulator from single electron in ray trace simulation.

ISBN 978-3-95450-174-8

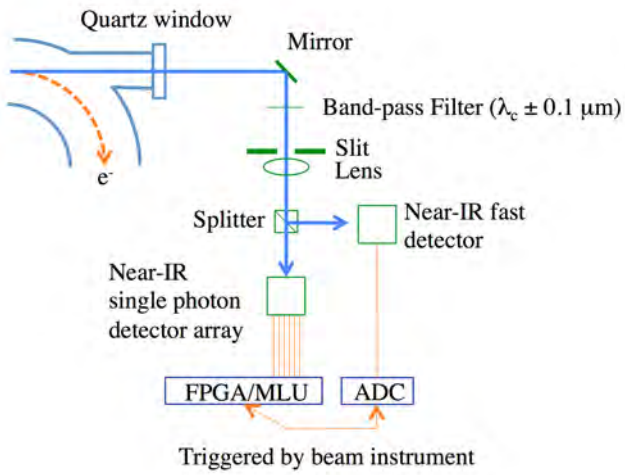

Figure 8: Schematic of beam diagnostic system.

ISBN 978-3-95450-174-8